

The Open-Source Cornell Spectrum Imager

Robert Hovden, Paul Cueva,* Julia A. Mundy, and David A. Muller

School of Applied and Engineering Physics, Cornell University, Ithaca, NY 14853

*pdc23@cornell.edu

Introduction

Hyperspectral imaging (also known as spectrum imaging) requires software for extracting the signatures present in every spectrum. However, commercial software available for spectrum analysis remains expensive, complicated, and often not transparent regarding the internal workings and approximations made. For user facilities, educational institutes, and other settings where multiple users on a single tool can be expected, the limited availability of software becomes the bottleneck to data analysis, user training, and throughput. The Cornell Spectrum Imager (CSI) was developed as a universal data analysis tool to be freely distributed, to run on all computers, and to minimize training. This is accomplished by using one simple interface for imaging, cathodoluminescence, Raman, Electron Energy Loss Spectroscopic (EELS), and EDX data analysis. This article demonstrates the CSI plugins for ImageJ by guiding you through the basic workflow for processing EELS maps.

Download, Install, and Execute

The software package, CSI, can be downloaded for Windows, Mac OS X, or Linux operating systems at: <http://code.google.com/p/cornell-spectrum-imager> (click on the downloads tab). To begin using the tool, it is easiest to download one of the installers for Windows (.exe) or Mac OS X (.dmg) that will take you through the installation. If you have an existing installation of ImageJ and understand how to edit and install plugins, the necessary CSI plugins are contained in the .zip file. ImageJ without CSI is freely available from the National Institutes of Health at: <http://rsb.info.nih.gov/ij/>

CSI can be launched under the *Applications* directory in Mac OS X or through the *Start Menu* in Windows. When the program loads, a menu bar with a variety of CSI shortcut icons will appear (Figure 1a). Because CSI is built on ImageJ, all of the functionality familiar to ImageJ users is also available—much of which is useful in processing spectral data. The tools provided by CSI can be found in the *Plugins>CSI* drop-down menu. CSI is currently distributed in 64-bit format, allowing substantial memory allocation. Users processing large datasets

will need to increase the memory available to CSI in the *Edit>Options>Memory & Threads* drop-down menu.

Open and View EELS Datasets

To load a spectral dataset, click on the open spectra shortcut icon (Figure 1a). It will handle .dm3, .ser, and other common file types—such as raw binary or tiff stacks. Alternatively, data can be loaded using DM3 Reader or TIA Reader in the *Plugins>CSI* drop-down menu, as well as options available under *File>Import*. Unfortunately, a DM4 reader is not yet available because Gatan does not currently provide information regarding this new file format.

Once your data have been opened, it becomes immediately browsable. A single EELS spectrum will appear as an intensity vs. energy plot, a linescan appears as an intensity plot of position vs. energy, and for 2D spectral maps a scrollbar allows you to browse the image at any specified energy (Figure 1d). As an example, a small atomic-resolution EELS map is provided in the */ImageJ/SampleData* directory. When scrolling through the energies of an EELS map, you may wish to toggle the auto-contrast button. This swaps between the default setting of automatically viewing each slice at its optimum contrast range or viewing all slices on the same intensity scale (a * at the end of the filename in the window indicates autoscaling is disabled).

When scrolling through the energy loss maps, the signal may be dominated by one or few hot pixels caused by cosmic

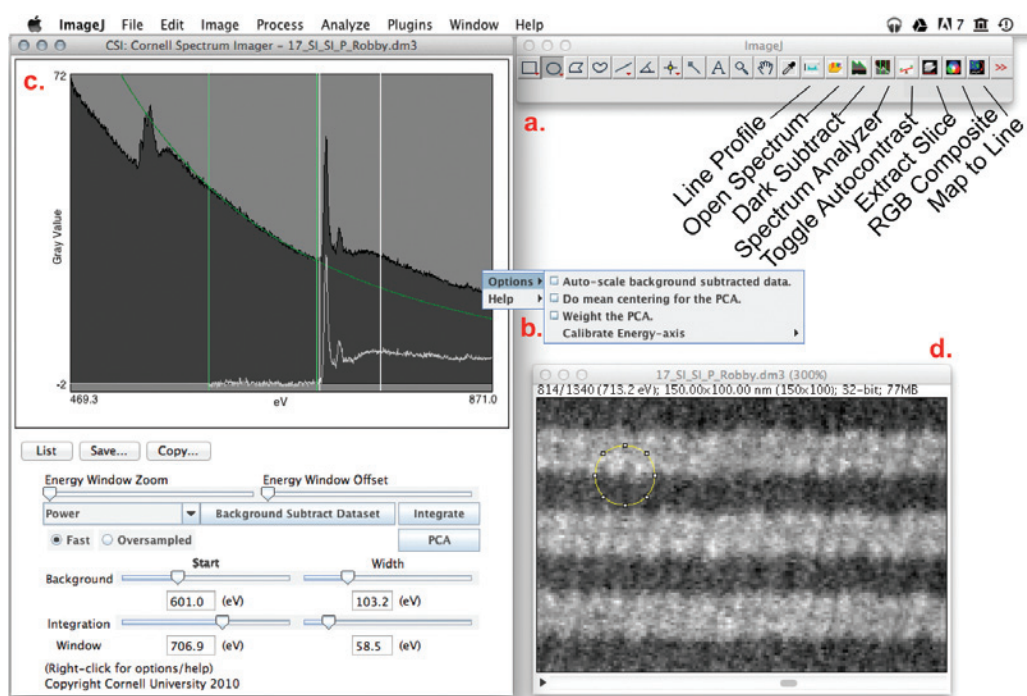




Figure 1: Screenshot of CSI software (v1.4) being used to analyze EELS spectral map data. (a) Shortcut icons for manipulating the dataset, (b) additional options menu, (c) spectrum analyzer showing background subtraction, and (d) the spectral map data displayed at a particular energy loss (scroll bar displays different energies).

rays or defects in the CCD. These outliers can be removed using *Process>Noise>Remove Outliers* in the drop-down menu. Light noise filtering will improve EELS analysis, but if the outlier threshold is set too low, the data will become median-filtered and spatial resolution will be lost. By removing hot pixels, image contrast of the raw data will be noticeably improved.

For specimens containing chemical edges with strong jump ratios, the constituent elements in the map become immediately apparent when scrolling across an edge energy onset. However, extracting a chemical map almost always requires removing the influence of the pre-edge background containing the tails of lower-energy edges and then integrating over the selected edge's energy range [1]. This is done within the Spectrum Analyzer window of CSI.

The Spectrum Analyzer

Detailed spectral data analysis is done within the Spectrum Analyzer window (Figure 1c). After your data have been loaded, you can open the analyzer with the  icon or under *Plugins>CSI>Spectrum Analyzer*.

The Spectrum Analyzer allows you to browse information along the spectroscopic axis—in this case, electron energy (eV). For a spectral map, you can select any pixel or average signal over a region of interest using the selection toolset .

The selected region need not be square—unique shapes can be generated to select nanoparticles, atomic interfaces, or semiconductor devices. When the selected region is moved, the displayed spectrum will be updated in real time. This is useful for finding elements present in a specimen, their changes in concentrations, and any fine structure changes that may occur across an interface. The *Energy Window Zoom* and *Energy Window Offset* sliders allow the user to look at specific energy windows with more detail. Fine adjustments to the energy window can be made by either typing in a specific energy in the textbox just below or clicking the slider marker and then using the left/right arrow keys.

If the spectral axis of a dataset needs recalibration, right-clicking on the spectrum analyzer allows access to *Calibrate Spectral Axis*. Users can calibrate by specifying the position of an identifiable feature in the spectrum, such as an ionization edge, and the channel size. Alternatively, the calibration can be accomplished by specifying the position of two features. Once a calibration approach is selected, sliders specify the energy position of the feature. Editable text boxes are used to set the feature's calibrated position or channel size. Changes are applied with the *Do Calibration* button.

Background Subtraction

Background extrapolation and subtraction is an integral part of EELS data analysis. This is accomplished within CSI by moving the *background start* and *width* slider bars in the Spectrum Analyzer window (Figure 1c). The corresponding background energy window is shown by two vertical green bars in the spectrum. Again, fine adjustments can be made with the left/right arrow keys or by entering specific energies in the related textbox.

Once an appropriate background window has been chosen, select the preferred fitting model by clicking on the drop-down menu just above the background sliders. Typically, this means changing the default value of *no fit* to the power law model, *power*. Additional fitting methods are


also provided for more advanced analysis and other types of spectral data. In particular, we have introduced a new fitting method termed Linear Combination of Power Laws (*LCPL* in the fitting menu) that provides a more stable background model by fitting two power laws with fixed exponents [2]. When spectral counts are low, LCPL outperforms traditional power-law modeling.

Immediately after a background model is selected, the background-subtracted spectrum is overlaid in white. You can scale-up this white background-subtracted spectrum by clicking *Auto-scale background subtracted data* in the advanced options menu (right-click anywhere on the Spectrum Analyzer window).

High-magnification spectral maps are often spatially oversampled. This is the case at atomic resolution where the pixel size is up to ten times smaller than the electron probe. For such scenarios, CSI can take advantage of the redundancy in a local background by spatially averaging the background with a gaussian described by the full-width-at-half-maximum. Click the *Oversampled* radio button and specify the probe's full-width-at-half maximum (FWHM) in the editable text box. Specifying a FWHM much larger than the spatial resolution can introduce artifacts such as blotching or ringing [2].

Clicking the *Background Subtract Dataset* button will produce a dataset with the corresponding background subtraction performed on every pixel—or alternatively, background subtraction and edge integration can be done in a single step with the *Integrate* button.

Extracting Chemical Maps

With the background window specified, select the *Integration Window* by moving the *Start* and *Width* sliders in the Spectrum Analyzer. The corresponding integration window is shown by two vertical white bars in the spectrum (Figure 1c). Clicking the *Integrate* button will apply the background subtraction and edge integration on every spectrum and produce either a line scan or a chemical map. If the linescan selection is made using the region of interest selection toolset, a linescan profile of chemical intensity will be produced (Figure 2). The process can be repeated over multiple edges and the resulting maps can be combined in an RGB overlay by clicking the  icon or *Image>Color>Stack to RGB* in the menu bar. Figure 3 shows an atomic-resolution RGB map extracted from 802 × 1024 (821,248) spectra [3].

PCA Analysis

One advanced analysis tool provided by CSI is its principal component analysis (PCA) functionality. CSI calculates the single-value decomposition over the selected integration window. If a background model has been specified, the calculation will first background subtract the data when it runs. Simply click the *PCA* button (Figure 1c) to see the eigenvalue maps, their corresponding eigenvectors, and the scree plot (Figure 4). PCA finds components that account for the most variability in the spectral dataset, which often corresponds to the most prominent phases or element associations. The eigenvalue tells you how “much” a particular component influences one particular spectrum. Thus, the technique can elucidate changes in the spectra that might be less obvious in the raw data [4–5]. For example, changes in fine structure may be contained in the 2nd or 3rd component in a PCA. The first component is restricted to describing the

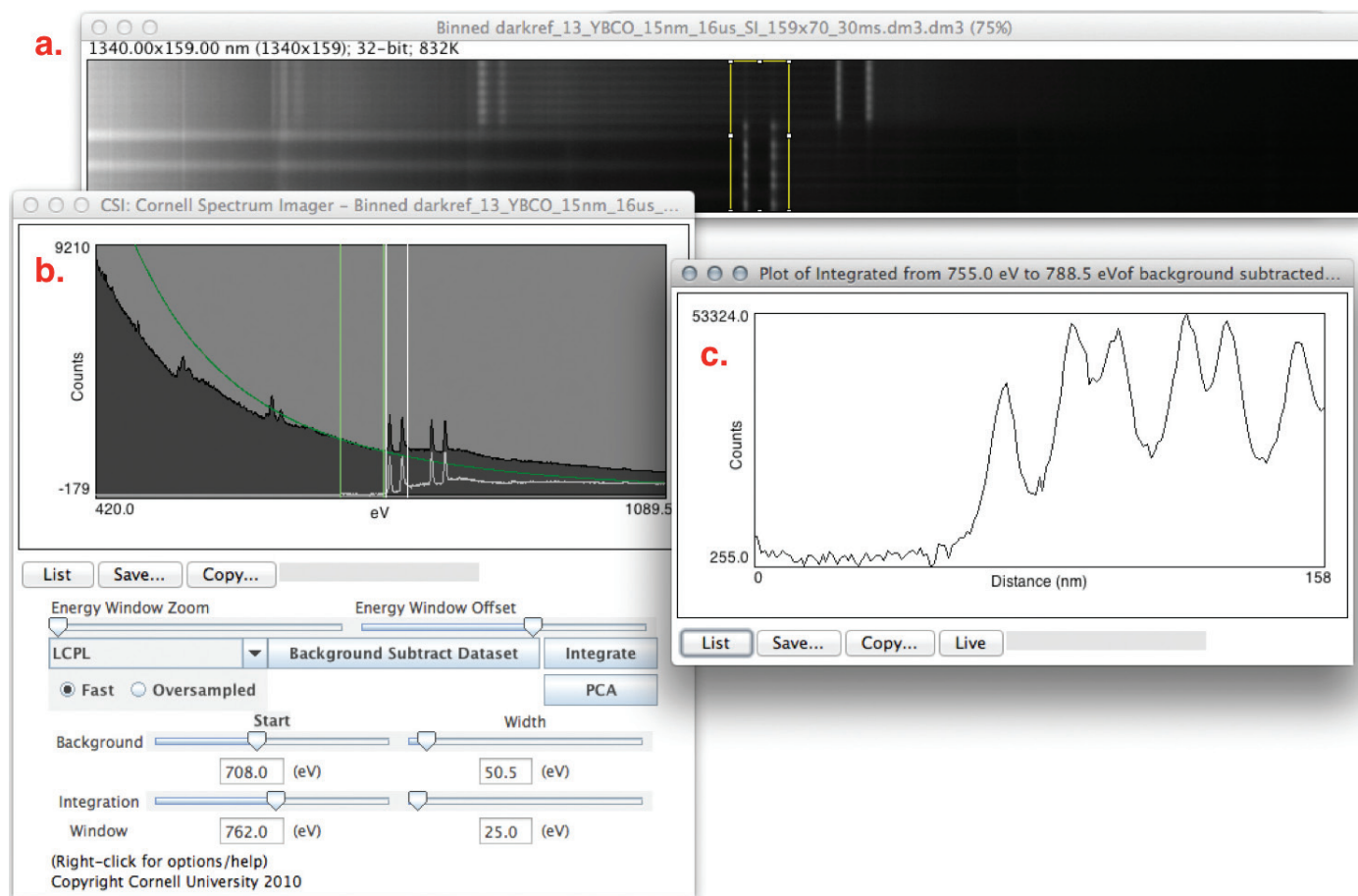


Figure 2: Screenshot of CSI being used to analyze an EELS spectrum spatial linescan. (a) The raw linescan data is displayed allowing selection in the spatial (vertical) direction. (b) The average EELS spectra over the selected region is displayed, and (c) background subtraction and integration can generate elemental intensity profiles.

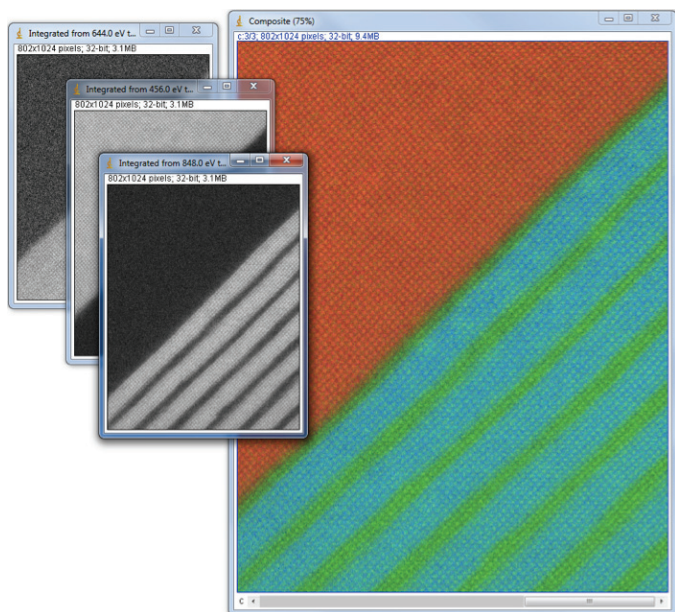


Figure 3: RGB composition of an atomic-resolution chemical map generated by CSI. The original single-element maps are shown (left), and the resulting RGB composite is shown in color (right). $(\text{LaMnO}_3)_6(\text{SrMnO}_3)_3$ superlattice on SrTiO_3 grown by Dr. Carolina Adamo and Prof. Darrell Schlom at Cornell University. Data acquired on NION UltraStem [3].

mean of the data unless the data are first mean-centered. By mean-centering the data (*Options > Do Mean Centering for PCA*), the PCA analysis will better characterize smaller changes in a spectrum [6]. The user can also perform a weighted PCA which, based on Poisson statistics, reduces the variance contributions from noisy regions in the spectrum (*Options > Weight the PCA*). The scree plot displays relative variance in the data represented by each component in order to help the user determine the appropriate number of components to interpret [2]. Although the intricacies of PCA and its interpretation are too complex for this tutorial, CSI allows easy implementation. PCA is a powerful inspection and analysis tool, however it should be used only for background-subtracted data because filtering of raw EELS data can drastically distort elemental distributions and EELS fine structure [7]. A comparison of the fine structure of the O-K edge shown in Figure 4 before and after weighted PCA is given in [8].

Discussion

Cornell's Microscopy Facilities are faced with several hundred users logging over 10,000 hours on several microanalysis instruments, making the purchase of proprietary commercial software for data analysis on each instrument cost-prohibitive. CSI was created to provide an open-source platform for intuitive, advanced approaches to data analysis

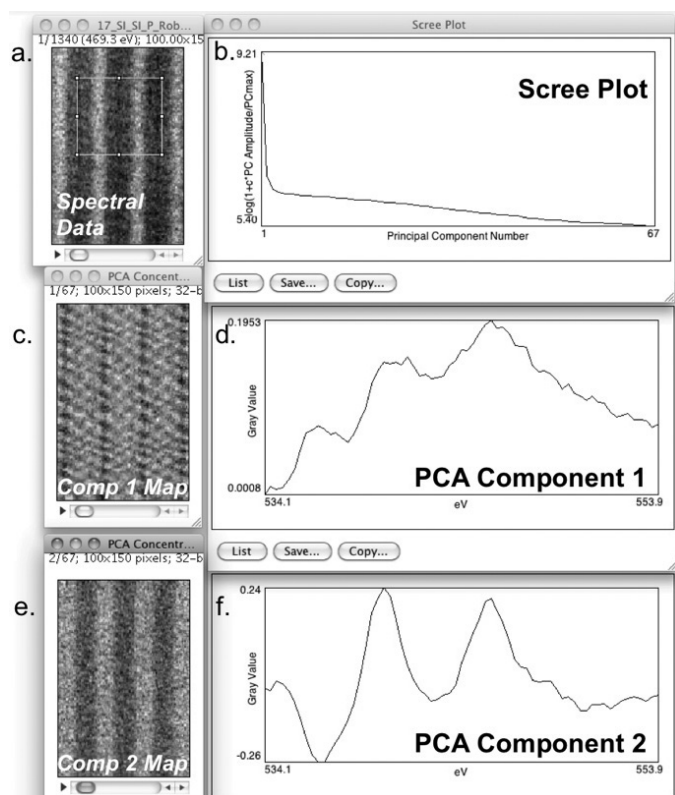


Figure 4: PCA of an EELS map (Oxygen K-Edge, LuFe_2O_4) showing the first two components. When running PCA on spectral data (a) in CSI, a map of all components (c or e), their shape (d or f), and a scree plot (b) is generated. The scree plot shows the declining relevance of higher-order PCA components in describing the dataset. PCA component 1 (d) is the mean O K-edge spectrum from the data set; the component 1 map (c) shows the intensity of this component in the dataset. From the scree plot (b) as well as the variation of component 2 map (e), we note that there is a physically different component 2 in the dataset, indicating that there are two different local bonding environments of O present. Although PCA component 2 (f) is not physically interpretable, the structure seen in its composition map (e) suggests local changes in the O-K fine structure. A detailed discussion of the data using other techniques is described in JA Mundy et al. [8]. PCA allows advanced analysis of fine structure changes and peak shifts in a spectrum. Sample grown by Charles Brooks and Prof. Darrell Schlom at Cornell University.

and processing of spectral data. Contained within CSI is a rich toolset for advanced spectral analysis beyond what is described in the present introductory tutorial. Although primarily developed for applications in electron microscopy, the open-source CSI and ImageJ platform provides an application programming interface for future algorithms or other spectroscopy communities. We encourage microscopists to use open-source software and promote open file format standards. Further documentation and updates are available at the Cornell Spectrum Imager website [9].

Acknowledgments

The authors thank Gregory Jefferis for his contributions to the DM3 reader ImageJ plugin as well as Peter Ercius for assistance with the multidimensional DM3 file formats. Without their understanding of the Gatan file formats, CSI would be greatly limited. Dr. Carolina Adamo, Charles Brooks, and Prof. Darrell Schlom provided exceptional specimens for EELS data analysis. We also acknowledge the hard work of Jo Verbeeck in developing EELSModel, another free advanced

tool for those wishing to process EELS data [10, 11]. Helpful feedback was also provided by Huolin L. Xin, Pinshane Huang, and Lena Fitting-Kourkoutis. Also thanks to Charles Lyman for his editorial eye. This work made use of the electron microscopy facility of the Cornell Center for Materials Research (DMR 1120296).

References

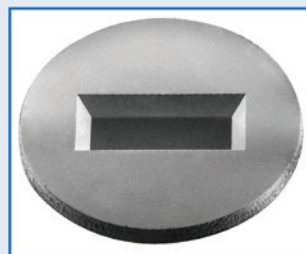
- [1] RF Egerton, *Electron Energy-Loss Spectroscopy in the Electron Microscope*, Springer, Boston, 2011.
- [2] P Cueva, R Hovden, JA Mundy, HL Xin, and DA Muller, *Microsc Microanal* 18 (2012) 667–75.
- [3] EJ Monkman, C Adamo, JA Mundy, DE Shai, JW Harter, D Shen, B Burganov, DA Muller, DG Schlom, and KM Shen, *Nature Materials* 11 (2012) 855–59.
- [4] M Bosman, M Watanabe, DTL Alexander, and VJ Keast, *Ultramicroscopy* 106 (2006) 24–32.
- [5] N Bonnet, *Ultramicroscopy* 77 (1999) 97–112.
- [6] T Pun, J Ellis, and M Eden, *J Microsc* 137 (1985) 93–100.
- [7] KJ Dudeck, M Couillard, S Lazar, C Dwyer, and GA Botton, *Micron* 43 (2012) 57–67.
- [8] JA Mundy, Q Mao, CM Brooks, DG Schlom, and DA Muller, *Appl Phys Lett* 101 (2012) 042907–11.
- [9] Cornell Spectrum Imager: <http://code.google.com/p/cornell-spectrum-imager/>.
- [10] J Verbeeck and S Van Aert, Model based quantification of EELS spectra. *Ultramicroscopy* 101 (2004) 207–24.
- [11] EELSModel: <http://www.eelsmodel.ua.ac.be/>.

MT

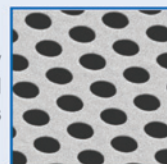
PELCO® Silicon Nitride & Silicon Dioxide Membranes

Next Generation SiN TEM Support Films

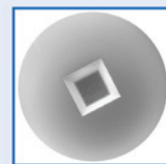
- Robust and clean 8, 15, 50 & 200nm SiN substrates
- ø3.0mm frame
- EasyGrip™ edges
- Free from debris
- Super flat 8, 15 and 40nm Silicon Dioxide Substrates



Holey
SiN
Substrates



Silicon
Dioxide
Substrates



TED PELLA, INC.
Microscopy Products for Science and Industry

sales@tedpella.com 800-237-3526 www.tedpella.com

Data Processing for Atomic Resolution Electron Energy Loss Spectroscopy

Paul Cueva,¹ Robert Hovden,^{1,*} Julia A. Mundy,¹ Huolin L. Xin,² and David A. Muller^{1,3}

¹*School of Applied and Engineering Physics, Cornell University, Ithaca, NY 14853, USA*

²*Department of Physics, Cornell University, Ithaca, NY 14853, USA*

³*Kavli Institute at Cornell for Nanoscale Science, Ithaca, NY 14853, USA*

Abstract: The high beam current and subangstrom resolution of aberration-corrected scanning transmission electron microscopes has enabled electron energy loss spectroscopy (EELS) mapping with atomic resolution. These spectral maps are often dose limited and spatially oversampled, leading to low counts/channel and are thus highly sensitive to errors in background estimation. However, by taking advantage of redundancy in the dataset map, one can improve background estimation and increase chemical sensitivity. We consider two such approaches—linear combination of power laws and local background averaging—that reduce background error and improve signal extraction. Principal component analysis (PCA) can also be used to analyze spectrum images, but the poor peak-to-background ratio in EELS can lead to serious artifacts if raw EELS data are PCA filtered. We identify common artifacts and discuss alternative approaches. These algorithms are implemented within the Cornell Spectrum Imager, an open source software package for spectroscopic analysis.

Key words: spectral mapping, EELS, STEM, aberration correction, PCA, software

INTRODUCTION

Elemental mapping via spectral analysis has proven extremely useful, especially in the field of scanning transmission electron microscopy (STEM). Techniques such as energy dispersive X ray (EDX), cathodoluminescence, and electron energy loss spectroscopy (EELS) all provide spatially resolved spectroscopic information. Spectral imaging, in which many spectra are acquired as the electron probe is rastered across the specimen, forms a two-dimensional spectral map—stored in a datacube of information (Jeanguillaume & Colliex, 1989; Hunt & Williams, 1991). The number of scanned points and signal-to-noise ratio (SNR) of a spectral image is greatly limited by the amount of signal, the instrument stability, and the user's time. Fortunately, a new generation of aberration-corrected electron microscopes has not only provided subangstrom lateral resolutions, but the large probe forming apertures (Batson et al., 2002; Okunishi et al., 2006; Bosman et al., 2007) and improved collection optics (Krivanek et al., 2008) also permit higher beam currents for rapid acquisition of spectroscopic signals down to atomic resolution (Muller et al., 2008; Muller, 2009; Botton et al., 2010). This has, in part, fueled the growing popularity and the acquisition of spectral images.

It is now possible to acquire thousands of spectra in a minute. As a result, spectral data are typically oversampled spatially. This is most clearly demonstrated with atomic resolution EELS mapping, where pixel dimensions are often ten times smaller than the probe size to provide a smooth and visually pleasing image, as well as reducing sensitivity to scan and high tension instabilities. Even at the nanometer

scale, changes in background behavior can be slowly varying, resulting in a spatially oversampled background signal. Approaches to exploiting the redundancy can range from simple smoothing and filtering to multivariate statistical analysis (Trebbia & Bonnet, 1990) and filtering, both of the background (Bosman et al., 2007) and the spectra (Bosman et al., 2006). This redundancy of information also offers opportunities for better background modeling—improving the size (in pixels), detection limits (in elemental concentration), and quality (in terms of SNR) of a spectral image (Liu & Brown, 1987). We find that improved background estimation can help reduce noise and artifacts not only for the obvious background extrapolations and interpolative models, but also for multivariate analysis. Here we consider two simple approaches for improved background estimation at low count rates—linear combination of power laws (LCPL) and local background averaging (LBA)—that can be combined with standard approaches to data processing including simple background extrapolation and signal integration, interpolative modeling of the background and edge combined (Verbeeck & Van Aert, 2004), and multivariate methods such as principal component analysis (PCA) (Trebbia & Bonnet, 1990; Bosman et al., 2006) and multivariate curve resolution (MCR) (Haaland et al., 2009).

Proper analysis of spectral data requires software for extracting the chemical signatures present in a spectrum. However, the commercial software available for spectrum analysis remains expensive, complicated, and often not transparent to the internal workings and approximations made. Worse, licensing terms generally restrict the software to a single computer tied to the data-acquisition microscope or a handful of machines. For user facilities, educational institutes, or any other setting where multiple users on a single

tool can be expected, the limited availability of software becomes the bottleneck to data analysis, user training, and throughput. Faced with several hundred users logging over 10,000 hours on our instruments at Cornell, we developed a universal data analysis tool that could be freely distributed, would run on all computers, and to minimize training would present the same user interface for imaging, EELS, and EDX data analysis. Our goal was software that could be run with minimal instruction or training—this meant ensuring all options needed for basic analysis were immediately visible to the user, and also limiting those options to avoid overwhelming a new user. This software package, the Cornell Spectrum Imager (CSI), freely downloadable from <http://code.google.com/p/cornell-spectrum-imager/> provides an open source platform for intuitive, advanced approaches to data analysis and processing of spectral images. It includes the background estimation and PCA algorithms discussed in this article, as well as a graphical interface for PCA.

METHODS AND RESULTS

Extracting EELS Core-Loss Edge

Electron energy loss spectroscopy, in which inelastically scattered electrons are sorted and detected according to their energies, provides detailed information about the chemical species, bonding, and structure of materials down to the atomic scale. Most often, the information of interest is contained in the core-loss energy edges. These edges appear in the EELS spectrum with a shape and energy onset uniquely defined by a specimen's excitation of core level electrons to the available density of states in the conduction band, and modified by the core-hole interaction. The edges lie on a background signal that can be produced by contributions due to valence excitations, core level excitations, plural scattering events, and combinations thereof. Despite the complexity, it has been shown that the background often follows an inverse power law (Egerton, 1975, 2011; Leapman, 2004), as seen in Figure 1.

The signal is most often obtained after the background has been modeled and subtracted over the edge of interest. The subtracted signal can then be integrated over a specified window (Joy & Maher, 1981). Alternatives to signal integration have also been demonstrated, most often in the form of component analysis. Component analysis, such as PCA, independent component analysis (ICA), or linear discriminant analysis (LDA), separates every spectrum in the dataset into additive subcomponents (Pearson, 1901; Friedman, 1989). The components can be used to characterize, or smooth, information in the core-loss region. Since the components are determined from the entire dataset, they take advantage of redundancy in the data and may provide better SNR than simple integration. However, many of the unbiased multivariate data analysis methods such as the popular PCA (Bonnet, 1999; Bosman et al., 2006) can fail to detect local behavior, such as interface states, under typical conditions, although they do lead to dramatic reduc-

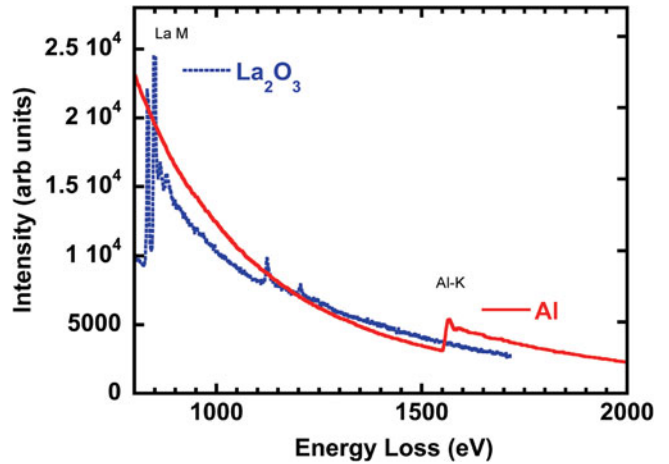


Figure 1. EELS spectra of the La-M and Al-K edges show the difference in power-law behavior that can occur in a specimen—the post La-M edge decay is clearly less rapid than the Al-K edge. Characterization of background behavior throughout a sample often requires multiple power laws.

tions in the apparent noise for the surrounding bulk material.

PCA is an optimal algorithm in the sense that it provides the least number of orthogonal vectors needed to capture a given percentage of the image variance. While PCA performs very well on X-ray spectral maps and secondary ion mass spectroscopy where the peak-to-background ratio is very high, it can produce serious but hard to recognize artifacts for EELS. The poor peak-to-background ratio in EELS means that much of that variance arises from changes in slope and shape of the background, rather than the edge of interest. The result is that the usual approach of using a scree plot to determine the number of significant components can grossly underestimate the number of significant components needed to describe the data. Figure 2 shows the consequences of PCA filtering raw data to remove noise—here retaining ten components, seven more than indicated necessary by the scree plot. The true structure of the Al-K edge is lost and replaced by an artifact that tracks the tails of the preceding La-M edge instead (Fig. 2). For energy dispersive spectrometry and secondary ion mass spectroscopy where backgrounds are very low compared to the signal, weighting the data by two-way scaling can improve the situation (Keenan & Kotula, 2004; Haaland et al., 2009).

Unfortunately for EELS, weighting often fails where most needed: in the limit of a vanishingly small signal on a large background, the scaling asymptotes back to the unweighted approximation. This effect is particularly pronounced when examining PCA filtered EELS fine structure (Fig. 3), which is often systematically distorted, with peaks shifting as much an electron volt. We have also found cases where the interface states themselves have been filtered away completely (Fig. 3c). The failure is not of PCA itself, but rather the global metric of total image variance. For instance, in an $N \times N$ pixel image, a line of interface states

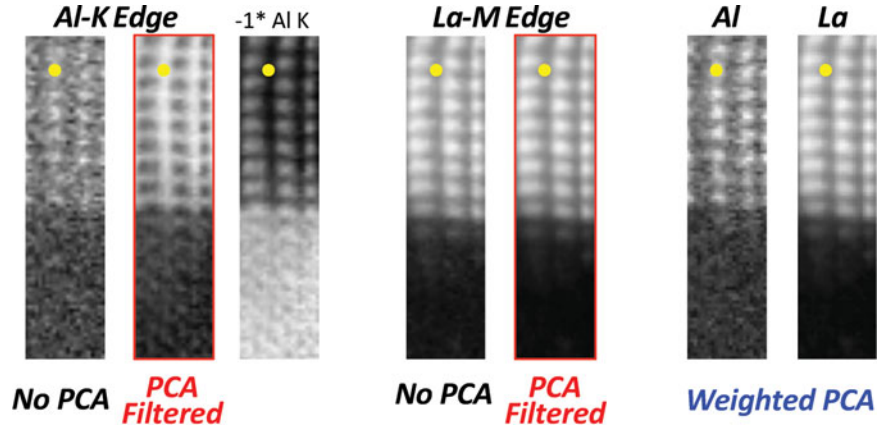


Figure 2. The Al-K and La-M edges recorded across a $\text{SrTiO}_3/\text{LaAlO}_3$ interface. The power-law subtracted and edge integration is applied to raw data (no PCA) and PCA-filtered (first ten components—seven more than suggested by the scree plot) datasets. While the unfiltered Al-K edge shows the Al lattice correctly, the PCA-filtered data show a contrast pattern that tracks the La-M edge contrast reversed, along with a false periodicity in the SrTiO_3 substrate. A weighted PCA (again ten components) is able to restore a more plausible Al-K map. However, as shown in Figure 3, the weighted PCA has introduced artifacts into the shape of the EELS fine structure and filtered out interface state.

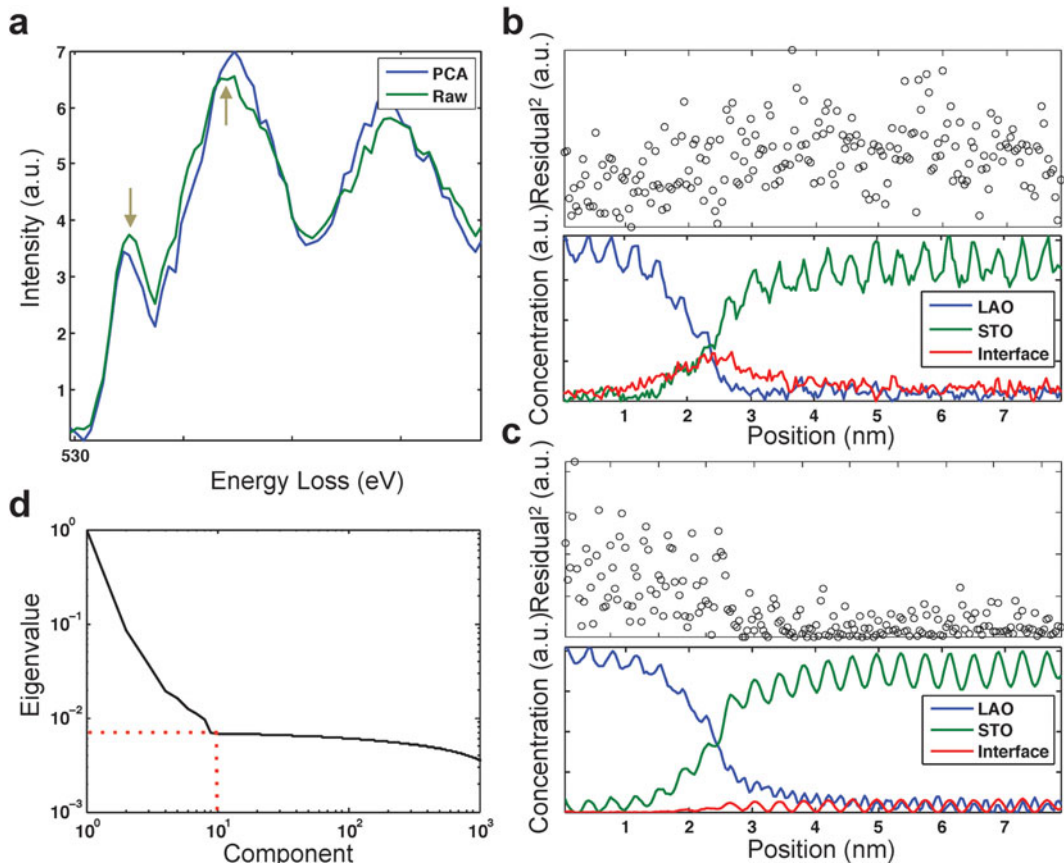


Figure 3. **a:** The O-K edge summed over 20 spectra recorded at a $\text{SrTiO}_3/\text{LaAlO}_3$ interface. If the raw data are 10-component PCA filtered prior to background subtraction, the shape of fine structure is altered, with the first and second peaks shifting strongly in opposite directions by -0.4 eV, $+0.4$ eV, respectively. **b, c:** Three-component MCR of the O-K edge across a $\text{SrTiO}_3/\text{LaAlO}_3$ interface. The MCR fit to the raw data (**b**) shows a clear interfacial component that is also apparent in the raw spectra, but is lost by weighted PCA filtering (**c**) the raw data prior to background subtraction. The MCR residuals appear well behaved (random) for the raw data (**b**) but structure remains in the filtered data (**c**). The weighted data (**c**) also displays unphysical intensity oscillations in the LAO and “interface” components. Scree plot (**d**) shows that almost all the variance is contained within the first nine components (dashed line).

only accounts for $1/N$ of the total image pixels. As $N \rightarrow \infty$, the fraction of image variance contained in the interface states tends to 0, and its PCA rank will drop below that of bulk noise components. Employing *a priori* knowledge of model-based approaches (Verbeeck & Van Aert, 2004), or local metrics such as spatially resolved residuals, often overcomes these problems. Local minimizations such as MCR (Haaland et al., 2009) can also be effective. Reducing changes in the EELS edge from background variation can be accomplished by subtracting a background fitted to the pre-edge region. This improves PCA performance by emphasizing only variance in principal components relating to the core-loss edge structure. Similar arguments may be made for ICA or LDA, suggesting that accurate background subtraction is important to many approaches to EELS signal analysis. In general, we would strongly recommend against PCA filtering raw EELS data, but rather to subtract the background before attempting any such analysis, and to keep in mind that any PCA filtered result is likely to be biased against detecting interfacial changes, especially if they are small.

Least-Squares Estimation

As a result of the relatively high background level, the accuracy of the background extrapolation directly—and significantly—affects the error in the signal of interest. Therefore, careful EELS analysis requires accurate characterization of the pre-edge signal and faithful background extrapolation over the EELS edge of interest. Traditionally, background extrapolation is accomplished by least-squares curve fitting of the pre-edge spectrum. Although most often edges will lie on a power law background (Egerton, 1975), situations may arise where regions are better described by another function—e.g., linear fits over small energy window when edges overlap (Rez, 1983) or exponential fits to low energy loss regions at moderate thicknesses. However, assuming the background can be modeled as a power law, we can express it as

$$b(E) = cE^{-r}.$$

Improving the background estimation error, and ultimately the SNR of the final extracted signal, is accomplished by reducing the variance in parameters c and r (Egerton, 1982). The background error will grow rapidly as the integration region becomes more distant from the fit region (Pun et al., 1985). This limits the integration range to be near the edge onset. Therefore, improving background fits has a twofold benefit for signal extraction by reducing the error in the background estimation and also enabling larger integration windows.

The most common implementation of a power law fit is a linear least-squares fit to the log-log transform of the experimental spectrum (Egerton, 2011). For point-by-point and line profile EELS maps, the counts per channel tend to be large, and this approach is usually well behaved. For two-dimensional EELS maps, the counts per channel can be very low. After dark correction of the spectra, it is not unusual to find zero or negative values. Such values are

outside the domain of the log transform and therefore cannot be fitted by this simple least-squares approach. Replacing such “bad” values with a positive definite constant, as is commonly done in standard software, will bias the fit, making it extremely unstable. In our own work on EELS maps of nanoparticles on thin and porous supports, this instability forced us to consider alternative approaches.

Linear Combination of Power Laws

For a given estimator, it is possible to improve the estimate of the background by exploiting prior knowledge of the dataset at hand—for instance, knowing that physical power law exponents, $-r_i$, should be negative (decaying). One intuitive approach is to use a LCPL. In this method, all backgrounds in a spectrum image are assumed to be accurately described by a LCPL:

$$b(E) = \sum_i c_i E^{-r_i}, \quad (1)$$

where i specifies the number of power laws being used, E is the energy, r_i is the specified power law parameter, and c_i is the scalar coefficient determined by the best fit to the background. The power law parameters r_i form the user-specified basis and must be chosen to best model the dataset of interest. For X-ray absorption spectroscopy, Victoreen (1943) demonstrated that the background can be accurately described by two fixed power laws. This spectroscopy is closely related to EELS, and in our experience it is often the case that backgrounds in an EELS spectrum image can be characterized by two power laws:

$$b(E) = c_1 E^{-r_1} + c_2 E^{-r_2}. \quad (2)$$

Thus, once appropriate power laws have been determined for the dataset, it is a linear least-squares minimization problem to determine the two scalar coefficients, c_1 and c_2 . This approach has the advantage of avoiding the log transforms of the experimental data needed for the simple power law fit and caused its failure at low count rates. While the dimensionality of the problem (two parameters) has not been reduced from a simple power law fit of the form cE^{-r} , it has greatly improved the stability of the system—in effect setting upper and lower bounds to the background’s power laws. The burden is upon the user to choose appropriate power law coefficients, which requires a little knowledge of the system, or dataset, at hand. For example, with X-ray absorption, a common choice for a physical basis is 3 to 4. However, because of plural scattering in the EELS signal, the coefficients are typically around 3, and we expect them to fall in the range between 0 and 4.

One may prefer to take a more generic approach to determining the power law coefficients for LCPL. This can be effectively done by choosing power laws from a histogram of the power law coefficients that have been fit to each background in the spectrum image. We found that choosing the decaying power law coefficients at the 5% and 95% extremes (or 20/80% if very noisy) of the dataset do well at describing all power law behavior in the spectrum image. In

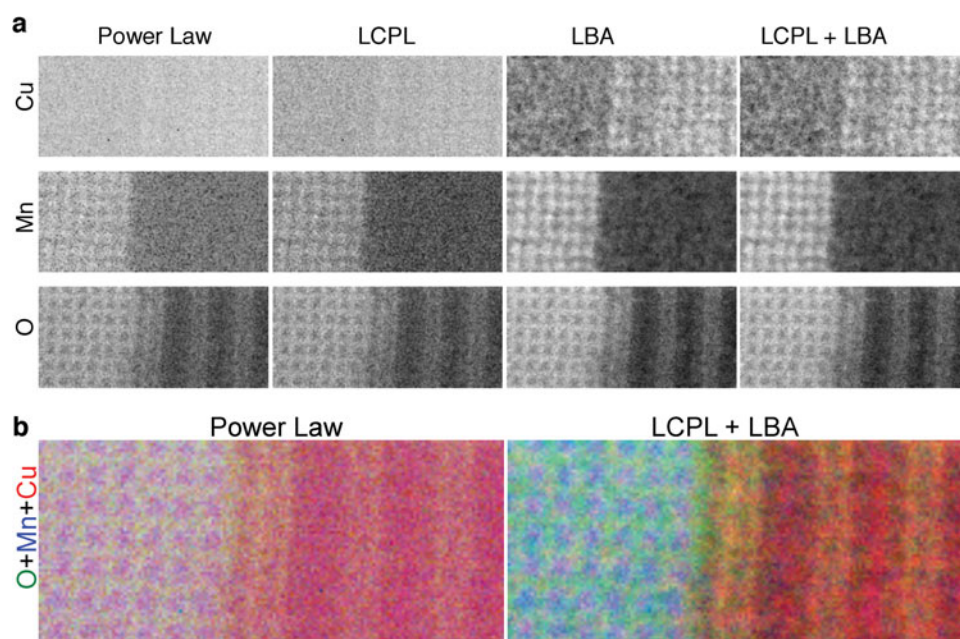


Figure 4. Atomic resolution chemical maps of an YBCO/manganite interface obtained from an EELS spectroscopic image. **a:** Elemental maps showing side by side comparison of different background subtraction methods **b:** RGB map displaying overall improvement from using traditional power law to LCPL with LBA. Data courtesy of Lena Fitting-Kourkoutis and Jak Chakalian.

this regard, one is considering the information of the entire dataset in order to process each individual spectrum. This global *a priori* information enables the improved background extrapolation.

The linear combination of two power laws appears robust over a range of specimens and edges—requiring only that sensible power laws are chosen. Picking the 5/95% extremes of all power law parameters in a spectral dataset provided results that were robust and free from noticeable artifacts. When applied to background subtracted atomic resolution EELS spectra, where the integrated core-loss edge provides a chemical concentration map, there is a small but noticeable improvement in the SNR. This can be seen in Figure 4a, for the Cu-L, Mn-L, and O-K edge maps. The improvements in SNR become more noticeable as the count rates drop—i.e., the most improvement for Cu then Mn then O.

Additionally, the LCPL behaves well at low count rates and in vacuum regions by preventing the spurious divergent exponents that result from taking the logarithm of zero or negative count channels in a simple linear least-squares power law estimation. Figure 5a shows what can happen when a simple power law fit is applied to a nanoparticle suspended over vacuum. Divergent extrapolations are often fit to the noise level in the vacuum region, resulting in wild extremes in the integrated intensities. LCPL corrects this, as visible in Figure 5b, by only allowing physically sensible negative power law coefficients. The method can potentially fail if the power laws are poorly chosen, or if a large energy window is selected in a sample with many regions of widely differing thickness. It is generally a good idea (for all approaches) to examine the background-subtracted dataset to

ensure the pre-edge region now fluctuates about zero, and there are no systematic deviations.

Local Background Averaging

LBA provides another approach to improved background modeling. Backgrounds that vary slowly with position can be averaged with those from neighboring spectra to obtain an accurate representation of the background at a given position. With this method, a background model is fit to the locally-averaged background signal at every position. The average of multiple spectra will have less Poisson noise than its constituent spectra. The reduced noise in the averaged background signal enables a more reliable background fit and extrapolation. Because the similarity in background behavior is more likely to decrease with radial distance from a given position, we implement a Gaussian averaging that is characterized by its full-width at half-maximum (FWHM). For a FWHM of 2 pixels, there will be approximately a two-fold improvement in the background's SNR. In fact, because the integrated average background counts grows with the square of averaging Gaussian FWHM and the background's SNR increases with square root of the counts (assuming Poisson statistics), there is a linear relationship that holds such that the LBA SNR improves approximately proportional to the FWHM of Gaussian. For even a FWHM of a few pixels, the dramatic increase in the background's SNR can have noticeable improvements in the background extrapolation and final signal. Note that this improvement in SNR is for the background estimate itself, not the edge of interest, which is still limited by the counting statistics of the spectrum. LBA will show improved results only when it is the error in background estimation that dominates the noise.

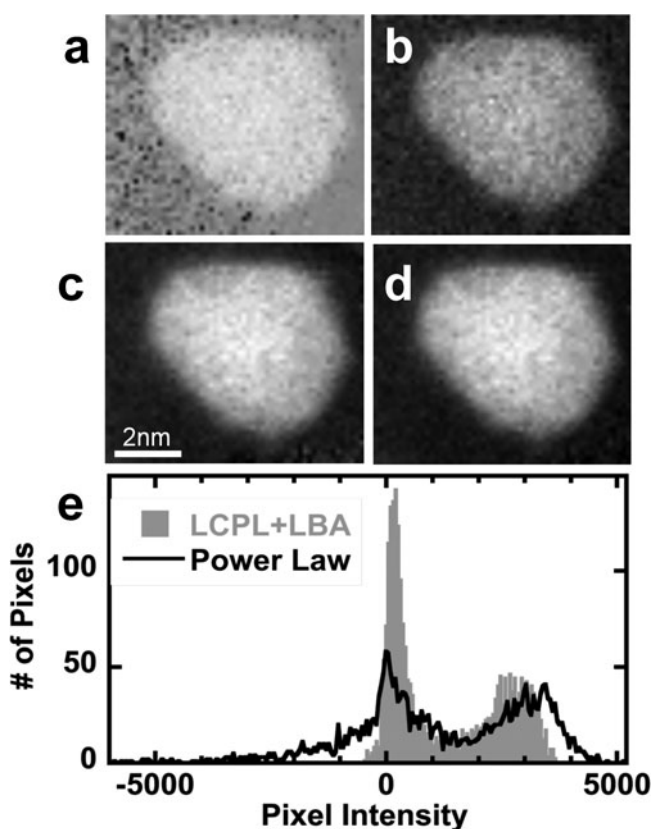


Figure 5. Different background subtraction algorithms on a Pt-M edge from a Pt₃Co nanoparticle. The peak/background ratio is good, but the number of counts per channel is low. (a) Power law fit, (b) linear combination of two power laws (LCPL), (c) 3-pixel radius LBA for the power law exponent, (d) combining both the LCPL of (b) and the LBA of (c), (e) histograms of image intensities, showing the reduced scatter of (d) compared to the basic power law (a).

However, if the radius of averaging extends over two dramatically different backgrounds, the algorithm begins to fail. This typically limits the averaging FWHM to a few pixels. Local averaging can easily create artifacts when significant changes in the background's power law behavior occurs spatially less than the FWHM of averaging—e.g., abrupt interfaces, nanoparticle edges, sample to vacuum transitions. However—as often is the case—when maps oversample with respect to changes in the background, local averaging can be used free of artifacts.

Atomic resolution EELS maps are often oversampled, with pixel dimensions smaller than the probes transfer limit. In this case, LBA works exceptionally well at estimating the background signal. When the core-loss edges are integrated to form a chemical map, local background averaging can provide a dramatic improvement in the image contrast and SNR. Figure 4a shows the improvement of local averaging over simple power law fitting and LCPL in an atomic resolution dataset. The local averaging provides a clearly visible atomic resolution Cu map that was previously lost in the noise. Although the Cu signal in Figure 4a is a particularly dramatic example of

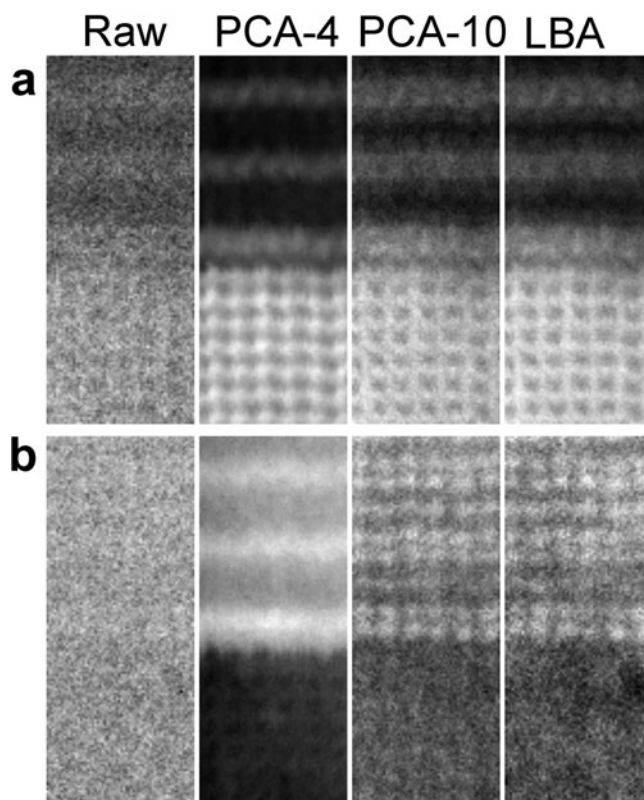


Figure 6. Comparison of noise reduction methods that exploit redundancy in the measured dataset for (a) the power-law-subtracted O-K and (b) Cu-L edges from the YBCO/manganite interface (Raw) and again simple power law fits after weighted PCA filtering with four (PCA4) and ten (PCA10) components, and finally the raw data after LBA and LCPL is applied instead (LBA). With four principal components, the maps do not reflect the physical positions of the atoms, while with ten components (four more than suggested by its scree plot), the PCA results comes closer to resembling the more plausible LBA/LCPL result.

how advantageous local averaging can be for atomic resolution images, the effects are still noticeable in other atomic maps (as seen in the Mn and O maps of Fig. 4). When compared to smoothing by weighted PCA with a sufficient number of components, LBA and PCA have converged to similar compositional results (Fig. 6), except LBA avoids the distortions to the EELS fine structure observed in PCA.

Despite being well suited for atomic resolution images, local background averaging can be applied to systems at other scales. Figure 5c shows how LBA improves the signal of a nanoparticle EELS map by reducing noise and increasing contrast. However, unlike atomic resolution images, which often sample beyond the probes contrast transfer limit, nm-resolution images are undersampled so there may be no correlation between neighboring pixels. Under these conditions it is often safer to instead smooth the original data prior to background correction. Rapid variations in the background can lead to artifacts in the LBA approach. One has to always be prudent when using LBA to characterize sharp interfaces at this scale. When dramatic changes in

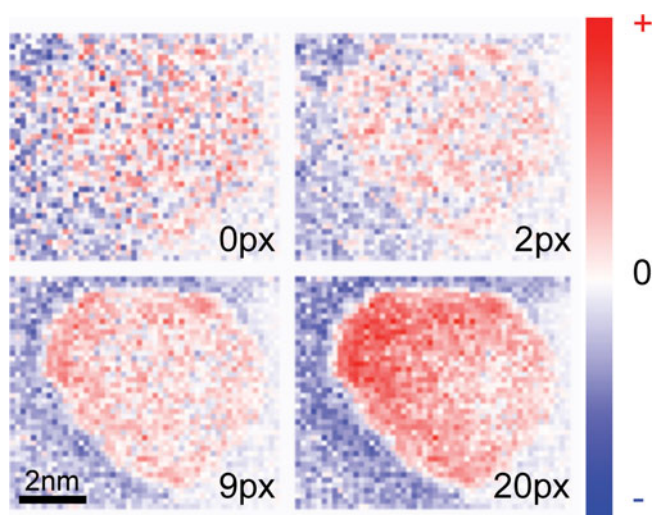


Figure 7. Map showing LBA integrated Pt-N edge intensity in a Pt_3Co particle on carbon support. The Pt-N edge has a much larger background compared to the Pt-M edge. Increasing the size of the averaging kernel can introduce ringing—here visible as a negative (blue) ring around the particle for the 9 and 20 pixel FWHM maps. The true background should be around zero (white). Such rings could be mistaken for an unphysical core-shell structure that is not present in the Pt-M edge shown in Figure 5.

background occur over regions larger than the FWHM of the Gaussian averaging, then the LBA signal is no longer a representative background. This usually occurs in the vicinity of interfaces—often the region of interest. For a nanoparticle, this occurs at the edges of the particles. Figure 7 shows the onset of edge artifacts with the FWHM of the Gaussian average is increased up to 20 pixels (0.133 nm/pixel). By a FWHM of 9 pixels, there is a noticeable ringing around the edge of the particle—a low intensity region just off the particle and a high intensity region just on the particle. This ringing is an artifact that can arise from LBA and may lead a researcher to reach incorrect conclusions about the core shell structure of their particle. In the case of LBA on nanoparticle shell structures, one must be cautious when making claims about features smaller than the FWHM of the local averaging.

DISCUSSION

Cornell Spectrum Imager

Accompanying this article, we present a free, open-source software tool for spectral analysis of EELS, EDX, or cathodoluminescence (CL) data—the Cornell Spectrum Imager (CSI) (Fig. 8). CSI can be downloaded from <http://code.google.com/p/cornell-spectrum-imager/>. CSI aims to provide an efficient, intuitive user interface that also includes unique features. Built as a plugin for the ImageJ platform, CSI offers an approachable graphical interface supported by standard image analysis software. Users on PC, Mac, or Linux can work with multigigabyte one-, two-, or three-dimensional datasets. In its current realization, CSI can read

DigitalMicrograph (.dm3), Emispec, image stack, or datacube files containing a single spectrum, line profile, or map. Once the data have been read into ImageJ, the spectrum analyzer allows the option of point, line, rectangle, circle, and free-hand region selection on spectrum images enables analysis of irregularly shaped features. CSI includes LCPL and local averaging for background modeling. Additional features currently include weighted and unweighted PCA that allow for smoothing and higher-level analysis of fine structure variations. CSI is optimized for generating single or composite chemical maps from three-dimensional spectral datasets, either by integration or principal components.

Alternative Background Estimation

When using very large energy windows, it is not correct to assume that the error in each channel is equal. This is especially the case for backgrounds in the first few hundred electron volts of a spectrum. To overcome this, iterative weighted least-squares approaches can be used to incorporate the changing in variance over the background (Pun et al., 1985). Furthermore, a maximum likelihood estimation was shown to outperform all least-squares estimation approaches, and the only noise source is from the Poisson statistics (Unser et al., 1987). In practice at very low count rates, the Gaussian readout noise can dominate and reduces the bias expected for least-squares fitting for the LCPL. The standard power law will still fail as the log-transform cannot properly handle negative contributions from the readout noise. Egerton (2002) has also discussed a two-window approach to improving background estimation. Although these techniques were not implemented with this work, they can readily be combined with LCPL and LBA. As CSI is as an open source project, it lends itself to public implementation of these algorithms.

CONCLUSIONS

The detection limits and SNRs of images extracted from spectroscopic mapping depend highly on the signal processing methods. This is especially true for core-loss EELS, in which pre-edge power law background modeling can greatly affect the accuracy and range of the extrapolated background. We have aimed to improve EELS background characterization by two approaches—both of which utilize *a priori* knowledge: linear combination of power laws and local background averaging. LCPL works well over a range of specimens, but is particularly useful when low background counts would normally lead to wildly fluctuating backgrounds. LBA works well when the background has been spatially oversampled. The two are not mutually exclusive and can be combined to give optimal results. They also avoid the distortions to the EELS fine structure observed with PCA. These algorithms, and others, have been implemented through open-source software based on the ImageJ platform. The CSI provides a modifiable and extendable EELS analysis toolset that is available, free, to the microscopy community.

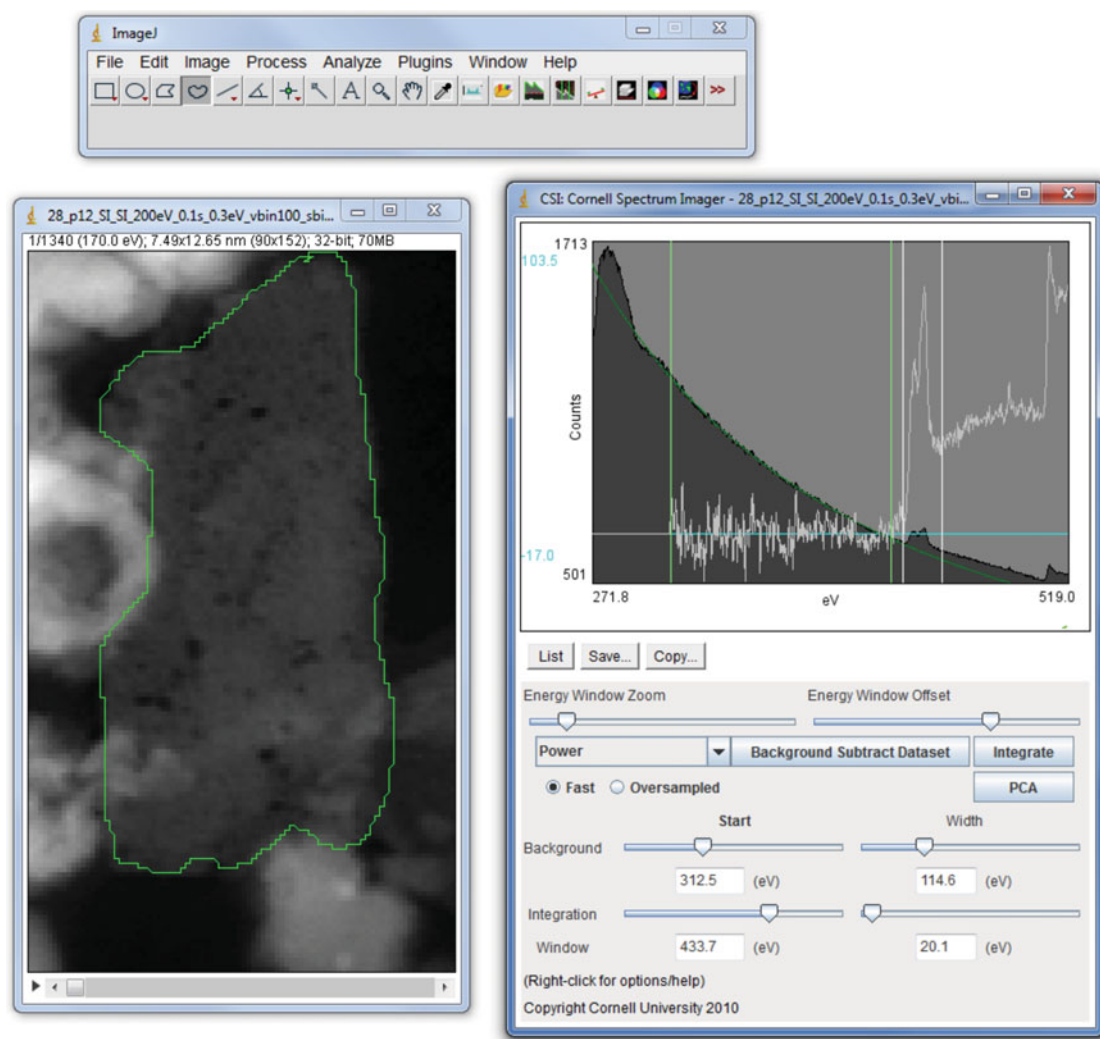


Figure 8. Screenshot of CSI performing analysis of a three-dimensional EELS dataset. Averaged energy loss spectrum (right, dark gray) from selected freehand region of dataset (left, green) is shown with power-law background extrapolation and autoscaled background-subtracted spectrum. By setting appropriate background and integration windows (right, vertical lines), one can immediately obtain a chemical map from the integrated intensity of each spectrum contained at every pixel.

ACKNOWLEDGMENTS

We would like to give particular thanks to Gregory Jefferis for his kind contributions to the DM3 reader ImageJ plugin as well as Peter Ercius for assistance with the multidimensional DM3 file formats. We also acknowledge helpful feedback from Pinshane Huang, Lena Fitting-Kourkoutis, and Earl Kirkland (Cornell) and Marion Stevens-Kalceff, Chee Chia, Stephen Joseph, and Paul Munroe (University of New South Wales) regarding the development of the Cornell Spectrum Imager. R.H. was supported by the Semiconductor Research Corporation and the Center for Nanoscale Systems, a National Science Foundation (NSF) Nanoscale Science and Engineering Center (NSF #EEC-0117770, 0646547). P.C. was supported by U.S. Department of Energy Basic Energy Science (DOE BES) Award #DE-SC0002334. H.L.X. and J.A.M. were supported by the Energy Materials Center at Cornell, an Energy Frontier Research Center (DOE

BES award #DE-SC0001086). J.A.M. was also supported by a National Defense Science and Engineering Graduate Fellowship. This work made use of the electron microscopy facility of the Cornell Center for Materials Research (CCMR) with support from the National Science Foundation Materials Research Science and Engineering Centers (MRSEC) program (DMR 1120296) and NSF IMR-0417392.

REFERENCES

- BATSON, P.E., DELLBY, N. & KRIVANEK, O.L. (2002). Sub-angstrom resolution using aberration corrected electron optics. *Nature* **418**, 617–620.
- BONNET, N. (1999). Extracting information from sequences of spatially resolved EELS spectra using multivariate statistical analysis. *Ultramicroscopy* **77**(3–4), 97–112.
- BOSMAN, M., KEAST, V., GARCIA-MUNOZ, J., FINDLAY, S. & ALLEN, L. (2007). Two-dimensional mapping of chemical information at atomic resolution. *Phys Rev Lett* **99**(8), 86102.

- BOSMAN, M., WATANABE, M., ALEXANDER, D.T.L. & KEAST, V.J. (2006). Mapping chemical and bonding information using multivariate analysis of electron energy-loss spectrum images. *Ultramicroscopy* **106**(11–12), 24–32.
- BOTTON, G. A., LAZAR, S. & DWYER, C. (2010). Elemental mapping at the atomic scale using low accelerating voltages. *Ultramicroscopy* **110**(8), 926–934.
- EGERTON, R. (2002). Improved background-fitting algorithms for ionization edges in electron energy-loss spectra. *Ultramicroscopy* **92**(2), 47–56.
- EGERTON, R.F. (1975). Inelastic-cattering of 80 keV electrons in amorphous carbon. *Philos Mag* **31**(1), 199–215.
- EGERTON, R.F. (1982). A revised expression for signal/noise ratio in EELS. *Ultramicroscopy* **9**, 387–390.
- EGERTON, R.F. (2011). *Electron Energy-Loss Spectroscopy in the Electron Microscope*. Boston, MA: Springer US.
- FRIEDMAN, J. (1989). Regularized discriminant analysis. *J Am Stat Assoc* **84**(405), 165–175.
- HAALAND, D.M., JONES, H.D.T., VAN BENTHEM, M.H., SINCLAIR, M.B., MELGAARD, D.K., STORK, C.L., PEDROSO, M.C., LIU, P., BRASIER, A.R., ANDREWS, N.L. & LIDKE, D.S. (2009). Hyperspectral confocal fluorescence imaging: Exploring alternative multivariate curve resolution approaches. *Appl Spectrosc* **63**(3), 271–279.
- HUNT, J.A. & WILLIAMS, D.B. (1991). Electron energy-loss spectrum-imaging. *Ultramicroscopy* **38**(1), 47–73.
- JEANGUILLAUME, C. & COLLIEX, C. (1989). Spectrum-image: The next step in EELS digital acquisition and processing. *Ultramicroscopy* **28**(1–4), 252–257.
- JOY, D.C. & MAHER, D.M. (1981). The quantitation of electron energy loss spectra. *J Microsc* **124**, 37–48.
- KEENAN, M.R. & KOTULA, P.G. (2004). Accounting for Poisson noise in the multivariate analysis of ToF-SIMS spectrum images. *Surf Interf Anal* **36**(3), 203–212.
- KRIVANEK, O.L., CORBIN, G.J., DELLBY, N., ELSTON, B.F., KEYSE, R.J., MURFITT, M.F., OWN, C.S., SZILAGYI, Z.S. & WOODRUFF, J.W. (2008). An electron microscope for the aberration-corrected era. *Ultramicroscopy* **108**(3), 179–195.
- LEAPMAN, R. (2004). Quantitative EELS analysis. In *Transmission Electron Energy Loss Spectrometry in Materials Science and the EELS Atlas*, Ahn, C.C. (Ed.), pp. 49–96. Weinheim, Germany: Wiley-VCH Verlag GmbH & Co.
- LIU, D.R. & BROWN, L.M. (1987). Influence of some practical factors on background extrapolation in EELS quantification. *J Microsc* **147**, 37–49.
- MULLER, D.A. (2009). Structure and bonding at the atomic scale by scanning transmission electron microscopy. *Nat Mater* **8**(4), 263–270.
- MULLER, D.A., FITTING KOURKOUTIS, L., MURFITT, M., SONG, J.H., HWANG, H.Y., SILCOX, J., DELLBY, N. & KRIVANEK, O.L. (2008). Atomic-scale chemical imaging of composition and bonding by aberration-corrected microscopy. *Science* **319**(5866), 1073–1076.
- OKUNISHI, E., SAWADA, H., KONDO, Y. & KERSKER, M. (2006). Atomic resolution elemental map of EELS with a Cs corrected STEM. *Microsc Microanal* **12**(S2), 1150–1151.
- PEARSON, K. (1901). On lines and planes of closest fit to systems of points in space. *Philos Mag* **2**(6), 559–572.
- PUN, T., ELLIS, J. & EDEN, M. (1985). Weighted least squares estimation of background in EELS imaging. *J Microsc* **137**, 93–100.
- REZ, P. (1983). Detection limits and error analysis in energy loss spectrometry. In *Microbeam Analysis*, Gooley, R. (Ed.), p. 153. San Francisco, CA: San Francisco Press.
- TREBBIA, P. & BONNET, N. (1990). EELS elemental mapping with unconventional methods, I. Theoretical basis: Image analysis with multivariate statistics and entropy concepts. *Ultramicroscopy* **34**, 165–178.
- UNSER, M., ELLIS, J., PUN, T. & EDEN, M. (1987). Optimal background estimation in EELS. *J Microsc* **145**, 245–256.
- VERBEECK, J. & VAN AERT, S. (2004). Model based quantification of EELS spectra. *Ultramicroscopy* **101**(2–4), 207–224.
- VICTOREEN, J.A. (1943). Probable X-ray mass absorption coefficients for wave-lengths shorter than the K critical absorption wave-length. *J Appl Phys* **14**(2), 95–102.